Supporting Information

Birnbaum et al. 10.1073/pnas.1420936111

SI Methods

Protein Construct Design, Expression, and Purification.

Expression of soluble LC13 TCR, CD3εδ, HLA-B8, and OKT3 Fab. The soluble ECDs of LC13 TCR, HLA-B8 (FLRGRAYGL peptide), and HLA-B4405 (EEYLKAWTF peptide) were expressed in *Escherichia coli* strain BL21.DE3 and refolded from inclusion bodies essentially as described previously (1). Production, purification, and generation of Fab fragments of the CD3ε-specific antibody OKT3 was performed as previously described (2). For expression in High Five insect cells, CD3ε and CD3δ chains (including the cysteine-rich stalk region) were cloned into a modified version of pFastbac dual downstream of the GP67 signal peptide and upstream of thrombin-cleavable leucine zippers. For purification, a His_6 tag was present at the C terminus of the CD3δ chain. CD3εδ was expressed and purified by nickel-affinity and size-exclusion chromatography as described for LC13 TCR–CD3εδ. To remove disulfide-linked heterodimers, a final hydrophobic interaction chromatography step using a HiTrap Phenyl column (GE Healthcare) was performed.

Expression and purification of full-length LC13 TCR–CD3 complex. Genes encoding the full-length sequences of the LC13 TCR (LC13α-LC13β) and CD3 (CD3ε-CD3δ-CD3γ-CD3ζ), in which each individual chain was separated by 2A-peptide consensus motifs as described for the 1G4 TCR, were cloned into the pMIG vector. For purification purposes, a streptavidin-binding peptide tag was introduced onto the C terminus of the LC13β chain. High-level expression of TCR–CD3 complex on 293T cells was achieved by two-step retroviral transduction, as described previously (3). First, 293T.CD3 cells were generated. In brief, 4 μg of pMIG-CD3 plasmids were combined with the packaging vectors pPAM-E (4 μg) and pVSV-g (2 μg) and cotransfected into 10^6 293T cells in a 10-cm dish with FuGENE 6 (Promega) as previously described (4). The transiently transfected 293T cells were further cultured for 5 d. During this time, the retrovirus-containing supernatant was collected twice daily and used to transduce fresh 293T cells in the presence of 6 μg/mL Polybrene. At the end of the transduction, 293T.CD3 cells were analyzed for coexpression of GFP. High-level GFP-expressing 293T cells were enriched by cell sorting. Second, individual pMIG-TCRs were introduced to 293T.CD3 cells via another round of transfection-transduction. TCR–CD3 cell surface expression in 293T.CD3.TCR cells was confirmed by antibody staining and analyzed by FACS. High-level TCR–CD3-expressing 293T.CD3.TCR cells were enriched by cell sorting using OKT3. 293T cells were detached from roller bottles using 10 mM Tris, pH 8, supplemented with 0.15 M NaCl (TBS) and 0.5 mM EDTA. Pelleted cells were subjected to repeated cycles of Dounce homogenization and washing with 3× TBS and 3 × 10 mM Tris plus 1 M NaCl. Enriched membranes were solubilized overnight in TBS plus 1% digitonin. Solubilized membrane proteins were loaded onto streptavidin-Sepharose columns (GE Healthcare), washed with TBS plus 0.1% digitonin, and eluted with TBS plus 0.1% digitonin and 350 μM biotin. TCR–CD3 complexes were further purified via immunoaffinity chromatography using the CD3ε-specific antibody BC3 linked to protein A Sepharose (GE Healthcare). Protein was eluted using Gentle Ag/Ab Elution buffer (Pierce) plus 0.1% digitonin and immediately buffer-exchanged into TBS plus 0.1% digitonin.

Expression and purification of full-length 1G4 TCR–CD3 complex. Initial small-scale cotitrations with various ratios of TCR and CD3 viruses were conducted on 1 mL of 293 cells at 1×10^6 cells per milliliter in a 12-well plate. Cells were stained 24–48 h after infection with an anti-human TCR antibody (clone IP26) and measured for surface expression with an Accuri C6 flow cytometer. The ratio that produced the highest mean fluorescence intensity (MFI) for TCR expression was used for preparative protein production.

Two hundred ninety-three cells were cultured to ∼1–2 × 10^6 cells per milliliter, treated with 10 mM sodium butyrate and infected with TCR and CD3 virus at the ratio determined for optimal expression, and allowed to incubate at 37 °C and 5% CO_2 for 36–48 h. A small aliquot of cells was stained with IP26 antibody to ensure good expression, then spun down at 300 × *g* for 10 min in a refrigerated centrifuge. Pelleted cells were washed with 1× PBS solution plus 1 mM EDTA plus protease inhibitors, then lysed on ice in 20 mM Hepes, pH 7.2, 1 mM EDTA, and protease inhibitors for ∼20 min. The lysed cells were then Dounce homogenized, pelleted with a high-speed spin (30,000 × *g* for 20 min at 4 °C), and resuspended in solubilization buffer (20 mM Hepes, pH 7.2, 500 mM NaCl, 20% glycerol, 30 mM imidazole, and protease inhibitors) containing 1% N-dodecyl-β-D-maltopyranoside (DDM) for 1–2 h at 4 °C. Insoluble material was removed via a high-speed spin (30,000 × *g* for 20 min at 4 °C), and the supernatant was incubated with Ni-NTA resin for 3 h at 4 °C. Ni-NTA resin was washed several times with solubilization buffer plus 0.1% DDM, then eluted from the resin in solubilization buffer plus 0.1% DDM and 300 mM imidazole.

To further purify the TCR–CD3 complex, the Ni-NTA affinity-purified material was incubated with Rho 1D4 antibody immobilized on agarose NHS resin (no. 26196; Pierce) or Fc-tagged NY-ESO-1-HLA-A2 (created as described later) immobilized on protein A resin for 2–3 h at 4 °C. The resin was washed in solubilization buffer plus 0.1% DDM, then resuspended in solubilization buffer plus 0.1% DDM and treated with ∼1:100 mass ratio of rhinovirus 3C protease overnight at 4 °C. Protease treatment liberated the complex from the resin while also removing the intracellular domains from each CD3 chain.

The supernatant and several washes of the resin were then pooled, concentrated using a 100-kD MWCO spin concentrator, and purified via size-exclusion chromatography by using a Superose 6 10/300 column in 20 mM Hepes, pH 7.2, 150 mM NaCl, and 0.02% DDM. Peak fractions were analyzed for presence of CD3 and pMHC (when purified via pMHC-Fc), as well as for complete CD3 intracellular domain cleavage, via Western blot by staining with anti-His or anti-Flag (for CD3) and anti-β2m (for MHC) antibodies.

Expression, labeling, and purification of HLA-A2-NY-ESO-1 (A2-ESO1). HLA-A2 was fused to human β2m and a structurally stabilized variant of the NY-ESO-1 peptide [SLLMWITQV, as described previously (5)] to create a peptide–β2m–MHC single-chain trimer MHC (sctMHC), designed with the Y84A MHC mutation to allow for the peptide–β2m linker as previously described (6), and synthesized as a codon-optimized gene for expression in insect cells (Genscript). The gene was then placed into a variant of the pAcGP67A vector that contained the gp67 signal sequence and a human IgG Fc region with a His_6 tag at the C terminus of the gene. A rhinovirus 3C protease site (LEVLFQGP) was placed between the sctMHC and the Fc tag. The construct was then cotransfected with baculosapphire DNA (no. 554756; BD Biosciences) in Sf9 cells to create recombinant baculovirus per the manufacturer's instructions, and amplified to P1 virus.

To express A2-ESO1, 2 L of High Five cells were infected with 2 mL/L of baculovirus and allowed to incubate at 28 °C for 48 h. The medium was then cleared of cells, conditioned with 100 mM Tris·HCl, pH 8.0, 5 mM $CaCl_2$, and 1 mM $NiCl_2$ for 15 min, and

cleared of the resulting precipitate via centrifugation. The media was then incubated with Ni-NTA resin (no. 30250; Qiagen) at room temperature for 3 h. The resin was washed with several column volumes of 1× HBS (10 mM Hepes, pH 7.2, 150 mM NaCl) plus 20 mM imidazole before being eluted in 1× HBS plus 200 mM imidazole. A2-ESO1 was concentrated with a 30-kD MWCO spin concentrator and purified via size-exclusion chromatography in 1× HBS on a Superdex 200 column (GE Healthcare).

If monomeric A2-ESO1 was desired, the protein was treated with 0.01 mass ratio of rhinovirus 3C protease and allowed to incubate at 4 °C overnight. The protein was then cleared of the Fc tag and any undigested material by passing it several times over a protein A agarose column. The flow-through, containing the monomeric A2-ESO1, was then repurified via size-exclusion chromatography as described earlier. To fluorescently label the A2-ESO1, purified sctMHC was treated with fluorescein-NHS (no. 53029; Pierce) and purified away from untreated dye as suggested by the manufacturer.

Expression and purification of soluble 1G4 TCR. The ECDs of the 1G4 TCR were placed in pAcGP67a vectors containing an acidic or basic leucine zipper at the C terminus of the 1G4β and 1G4α chains, respectively, essentially as previously described (7). Baculoviruses were created as described earlier for A2-ESO1, and then the 1G4β and 1G4α were cotitered in 2-mL cultures to determine the optimal virus ratio for 1:1 expression of both TCR chains. The protein was then expressed and purified as described for A2-ESO, with the imidazole-eluted protein treated with rhinovirus 3C protease to remove the leucine zippers. Protein was then purified via size-exclusion chromatography on a Superdex 200 column.

Expression, purification, and labeling of anti-CD3 Fab (UCHT1). The sequences of the variable domains of UCHT1 were obtained from the previously solved UCHT1–CD3 structure (8). We then appended the mouse κ-chain constant region to the V_L and the IgG2a C_{H1} domain to the V_H regions of UCHT1 to create a Fab that would form a disulfide bond. The UCHT1 light chain construct was cloned into pAcGP67A, whereas the heavy-chain construct was fused to the N terminus of human IgG Fc with a rhinovirus 3C protease site as described earlier. The constructs were transfected to create baculovirus, titrated, expressed, and purified as described earlier for the soluble 1G4 TCR. To generate Fab, the purified material was cleaved with 3C protease and cleared with protein A resin as described earlier to create monovalent A2-ESO. To fluorescently label the UCHT1 Fab, purified Fab was treated with fluorescein-NHS (no. 53029; Pierce) and purified away from untreated dye as suggested by the manufacturer.

Purification of 1G4-A2-ESO-CD3-UCHT1 membrane-bound construct. Before final purification via size-exclusion chromatography on a Superose 6 column as described earlier, membrane-bound 1G4–A2–ESO–CD3 complex was mixed in a ∼1:30 ratio with UCHT1 Fab (purified as described earlier and buffer-exchanged into 1× HBS buffer containing 0.02% DDM) and copurified via size-exclusion chromatography conducted at 4 °C to limit dissociation of the Fab. The material was analyzed for Fab by Western blotting by using an anti-mouse secondary antibody.

MALLS. Samples were run over a Superdex-200 10/300 size-exclusion column in 10 mM Tris, pH 8, containing 150 mM NaCl. The eluate was passed through a Wyatt EOS 18-angle laser photometer coupled to a Wyatt Optilab rEX refractive index detector, and the molecular mass moments were analyzed by using Astra 6.1.

Surface Plasmon Resonance. Surface plasmon resonance experiments were conducted at 25 °C on a BIAcore 3000 instrument using 10 mM Tris, pH 8, containing 150 mM NaCl, and 0.005% surfactant P20 with 1% BSA to prevent nonspecific binding. The human MHC-I–specific monoclonal antibody W6/32 (9) was coupled to a CM5 chip by using standard amine coupling. The experiment was conducted essentially as described previously (10) with LC13 TCR or LC13 TCR–CD3εδ as the analyte at a concentration range of 0.1–10 μM. Steady-state analysis was performed by using BIAevaluation version 3.1.

SAXS. Data were collected by using a single camera length with a 2-m (for LC13-CD3εδ+OKT3) or 1-m (for all others) sample-to-detector distance to cover a momentum transfer interval of 0.013 $Å^{-1} < q < 0.3\ Å^{-1}$ or $0.011\ Å^{-1} < q < 0.63\ Å^{-1}$, respectively. The modulus of the momentum transfer is defined as $q = 4\pi\sin(\theta/\lambda)$, where 2θ is the scattering angle and λ is the wavelength. Scattering images were radially averaged and blank-subtracted by using in house software. For non–gel-filtered samples, molecular mass estimates were obtained by extrapolating scattering intensity to zero angle and normalizing relative to known concentrations of BSA. All samples were judged to be free of aggregation on the basis of the linearity of Guinier plots. The R_g and the pairwise intraparticle distance distribution function were determined by using GNOM (11). Ab initio models were generated by using DAMMIF (12). At least 10 independent DAMMIF runs were aligned, combined, and filtered to generate a final model that retained the most consistent features by using the DAMMAVER package. The normalized spatial discrepancies between individual DAMMIF models were 0.69–1.01 (HLA-B8, 2 mg/mL), 0.65–1.05 (CD3εδ, 1.4 mg/mL), 1.11–1.24 (LC13, 7 mg/mL), 0.98–1.16 (OKT3, 2 mg/mL), 0.69–0.85 (LC13-CD3εδ, 6 mg/mL), 0.94–1.15 (LC13-CD3εδ plus OKT3), and 0.82–1.08 (LC13-CD3εδ plus HLA-B44). Typical χ^2 values indicating the fit of individual DAMMIF models to the SAXS data were 0.8 (HLA-B8, 2 mg/mL), 0.61 (CD3εδ, 1.4 mg/mL), 0.64 (LC13, 7 mg/mL), 0.8 (OKT3, 2 mg/mL), 0.8 (LC13–CD3εδ, 6 mg/mL), 0.77 (LC13–CD3εδ plus OKT3), and 0.52 (LC13–CD3εδ plus HLA-B44). Fitting of high-resolution models of LC13 [Protein Data Bank (PDB) ID code 1KGC)], CD3εδ (PDB ID code 1XIW), OKT3 (PDB ID code 1SY6), and HLA-B8 (PDB ID code 1MI5) to the raw SAXS data was performed by using Crysol (13) and resulted in the following χ^2 values: CD3εδ (2.7), HLA-B8 (0.72), LC13 (1.2), and OKT3 (1.18). CORAL (14) modeling for the unliganded LC13–CD3εδ was performed by using the following subunits as rigid bodies: LC13, CD3εδ, and the heterotrimeric coiled-coil domain (PDB ID code 1BB1). The residues present in the TCR–CD3εδ construct but absent in the available crystal structures (12 residues at the N terminus of CD3ε; 4, 6, and 26 residues located between the N terminus of the coiled-coil subunit and the C terminus of CD3ε, CD3δ, and the LC13α chain, respectively; and 16 residues at the C terminus of the LC13β chain) were modeled as dummy atoms. For modeling LC13–CD3εδ bound to OKT3, a model for OKT3–CD3εδ was generated by superimposing the crystal structure of CD3εδ (PDB ID code 1XIW) onto the CD3ε chain of the OKT3–CD3εγ complex (PDB ID code 1SY6) and inputting this model into CORAL in place of unliganded CD3εδ. For modeling LC13–CD3εδ bound to HLA-B44, the unliganded LC13 subunit was replaced with the LC13–HLA-B44 complex (PDB ID code 3KPR). Typical χ^2 values describing the fit of the CORAL models to the SAXS data were 6.55 (unliganded TCR–CD3εδ), 0.87 (TCR–CD3εδ plus OKT3), and 1.2 (TCR–CD3εδ plus HLA-B44).

EM Image Processing. BOXER, the display program associated with the EMAN (electron micrograph analysis) software package (15), was used to interactively select 12,093 1G4 TCR–MHC particles from 155 CCD images, 25,804 1G4 TCR–CD3–MHC particles from 362 CCD images, and 19,652 1G4 TCR–CD3–MHC–anti-CD3 Fab particles from 610 CCD images. The SPIDER (system for processing image data from electron microscopy and related fields) software package (16) was used to window the particles into 120 × 120-pixel images for the TCR–MHC complex, and 200 × 200-pixel images for the TCR–CD3–MHC and TCR–CD3–MHC–anti-CD3 Fab complexes. To perform iterative stable alignment and clustering (ISAC) (17)

in SPARX (single particle analysis for resolution extension) (18), the size of the particle images was reduced to 64 × 64 pixels, and the particles were prealigned and centered. ISAC was run on the Orchestra High Performance Compute Cluster at Harvard Medical School (rc.hms.harvard.edu), specifying 50 images per group and a pixel error of 0.7 for the TCR–MHC complex, and 200 images per group and a pixel error of 2 for the TCR–CD3–MHC and TCR–CD3–MHC–anti-CD3 Fab complexes. For the TCR–MHC complex, seven generations yielded 107 averages that accounted for 1,563 particles (~13% of the entire data set). For the TCR–CD3–MHC complex, 17 generations yielded 175 averages that accounted for 4,035 particles (~16% of the entire data set). For the TCR–CD3–MHC–anti-CD3 Fab complex, 14 generations yielded 171 averages that accounted for 4,315 particles (~22% of the entire data set). Averages of these classes were then calculated by using the original 120 × 120-pixel or 200 × 200-pixel images. The particles were also subjected to 10 cycles of multireference alignment in SPIDER to ensure that the ISAC averages are representative of the entire data set. Each round of multireference alignment was followed by K-means classification, specifying 100 output classes for the TCR–MHC complex and 200 output classes for the TCR–CD3–MHC and TCR–CD3–MHC–anti-CD3 Fab complexes (Fig. S8). For LC13–CD3, particles were windowed into 18 × 18 nm boxes and subjected to six rounds of multireference alignment by using EMAN 2.07.

To compare the class averages of the TCR–MHC complex with the crystal structure (PDB ID code 2P5E) (19), the crystal structure was Fourier-transformed, filtered to 20 Å with a Butterworth low-pass filter, and transformed back. Evenly spaced projections were calculated at 4° intervals and subjected to 10 cycles of alignment with masked EM class averages. The five class averages with the highest cross-correlation and the corresponding projections from the model are presented in Fig. S9.

To create the class-average video loops, the 2D averages were centered and aligned to each other by using the SPARX command "sxali2d.py," selecting one average as reference for alignment. The averages were then sorted according to decreasing cross-correlation by using the SPARX command "sxprocess.py" with the option "order."

1. Clements CS, et al. (2002) The production, purification and crystallization of a soluble heterodimeric form of a highly selected T-cell receptor in its unliganded and liganded state. *Acta Crystallogr D Biol Crystallogr* 58(pt 12):2131–2134.
2. Dunstone MA, et al. (2004) The production and purification of the human T-cell receptors, the CD3epsilongamma and CD3epsilondelta heterodimers: Complex formation and crystallization with OKT3, a therapeutic monoclonal antibody. *Acta Crystallogr D Biol Crystallogr* 60(pt 8):1425–1428.
3. Beddoe T, et al. (2009) Antigen ligation triggers a conformational change within the constant domain of the alphabeta T cell receptor. *Immunity* 30(6):777–788.
4. Holst J, et al. (2006) Generation of T-cell receptor retrogenic mice. *Nat Protoc* 1(1):406–417.
5. Chen JL, et al. (2005) Structural and kinetic basis for heightened immunogenicity of T cell vaccines. *J Exp Med* 201(8):1243–1255.
6. Mitaksov V, et al. (2007) Structural engineering of pMHC reagents for T cell vaccines and diagnostics. *Chem Biol* 14(8):909–922.
7. Birnbaum ME, et al. (2014) Deconstructing the peptide-MHC specificity of T cell recognition. *Cell* 157(5):1073–1087.
8. Arnett KL, Harrison SC, Wiley DC (2004) Crystal structure of a human CD3-epsilon/delta dimer in complex with a UCHT1 single-chain antibody fragment. *Proc Natl Acad Sci USA* 101(46):16268–16273.
9. Parham P, Barnstable CJ, Bodmer WF (1979) Use of a monoclonal antibody (W6/32) in structural studies of HLA-A,B,C, antigens. *J Immunol* 123(1):342–349.
10. Borg NA, et al. (2005) The CDR3 regions of an immunodominant T cell receptor dictate the 'energetic landscape' of peptide-MHC recognition. *Nat Immunol* 6(2):171–180.
11. Semenyuk AV, Svergun DI (1991) GNOM - a program package for small-angle scattering data processing. *J Appl Cryst* 24:537–540.
12. Franke D, Svergun DI (2009) DAMMIF, a program for rapid ab-initio shape determination in small-angle scattering. *J Appl Cryst* 42:342–346.
13. Svergun DI, Barberato C, Koch MHJ (1995) CRYSOL– a program to evaluate x-ray solution scattering of biological macromolecules from atomic coordinates. *J Appl Cryst* 28:768–773.
14. Petoukhov MV, et al. (2012) New developments in the ATSAS program package for small-angle scattering data analysis. *J Appl Cryst* 45:342–350.
15. Ludtke SJ, Baldwin PR, Chiu W (1999) EMAN: Semiautomated software for high-resolution single-particle reconstructions. *J Struct Biol* 128(1):82–97.
16. Frank J, et al. (1996) SPIDER and WEB: processing and visualization of images in 3D electron microscopy and related fields. *J Struct Biol* 116(1):190–199.
17. Yang Z, Fang J, Chittuluru J, Asturias FJ, Penczek PA (2012) Iterative stable alignment and clustering of 2D transmission electron microscope images. *Structure* 20(2): 237–247.
18. Hohn M, et al. (2007) SPARX, a new environment for cryo-EM image processing. *J Struct Biol* 157(1):47–55.
19. Sami M, et al. (2007) Crystal structures of high affinity human T-cell receptors bound to peptide major histocompatibility complex reveal native diagonal binding geometry. *Protein Eng Des Sel* 20(8):397–403.

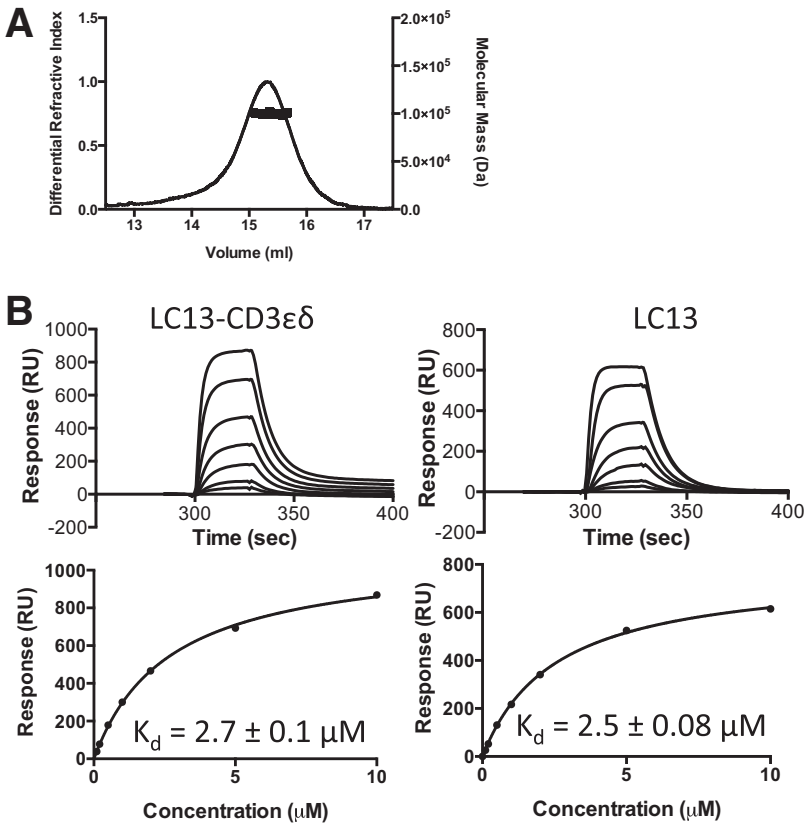

Fig. S1. Characterization of the LC13 TCR–CD3εδ complex. (*A*) The refractive index (thin line) of LC13 TCR–CD3εδ measured during size-exclusion chromatography is shown along with the molecular mass (thick line) calculated from simultaneous MALLS analysis. (*B*) Surface plasmon resonance sensograms (*Top*) and equilibrium binding curves (*Bottom*) are shown for LC13 TCR–CD3εδ (*Left*) and LC13 TCR (*Right*) binding to HLA-B44.

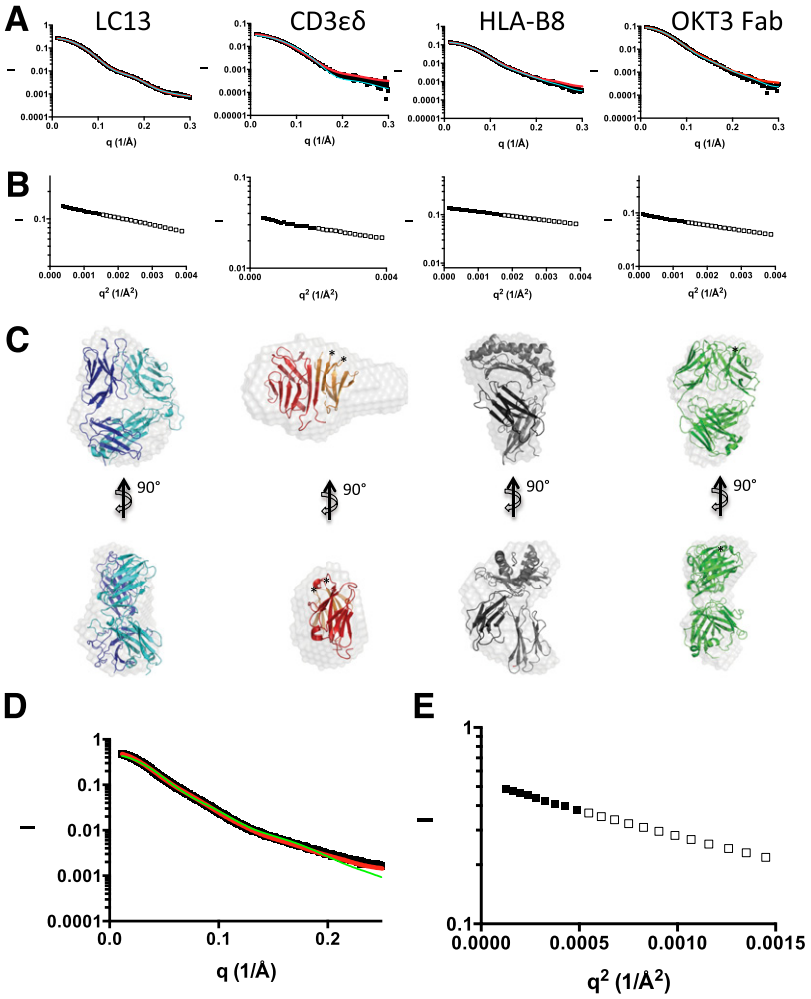

Fig. S2. SAXS data for individual protein components. Scattering curves (*A*) and Guinier plots (*B*) are shown for the ECDs of the LC13 TCR (7.3 mg/mL), CD3εδ (1.4 mg/mL), HLA-B8 (2 mg/mL), and OKT3 Fab fragment (2 mg/mL). In *B*, the plot should be linear for values of $q \leq 1/R_g$ (filled squares). In *C*, the SAXS-derived ab initio models (gray) are shown overlaid with the corresponding crystal structures (ribbons colored as in Fig. 1) in two orientations. The theoretical scattering curves computed from a representative ab initio model (red) and the crystal structures (blue) are shown overlaid with those determined experimentally (black squares) in *A*. (*D*) Fit of representative ab initio (red line) and CORAL (green line) models to SAXS data of LC13–CD3εδ at 6 mg/mL (black squares). (*E*) The low-angle region of the SAXS data in *D* is shown in the form of a Guinier plot, which should be linear for values of $q \leq 1/R_g$ (filled squares).

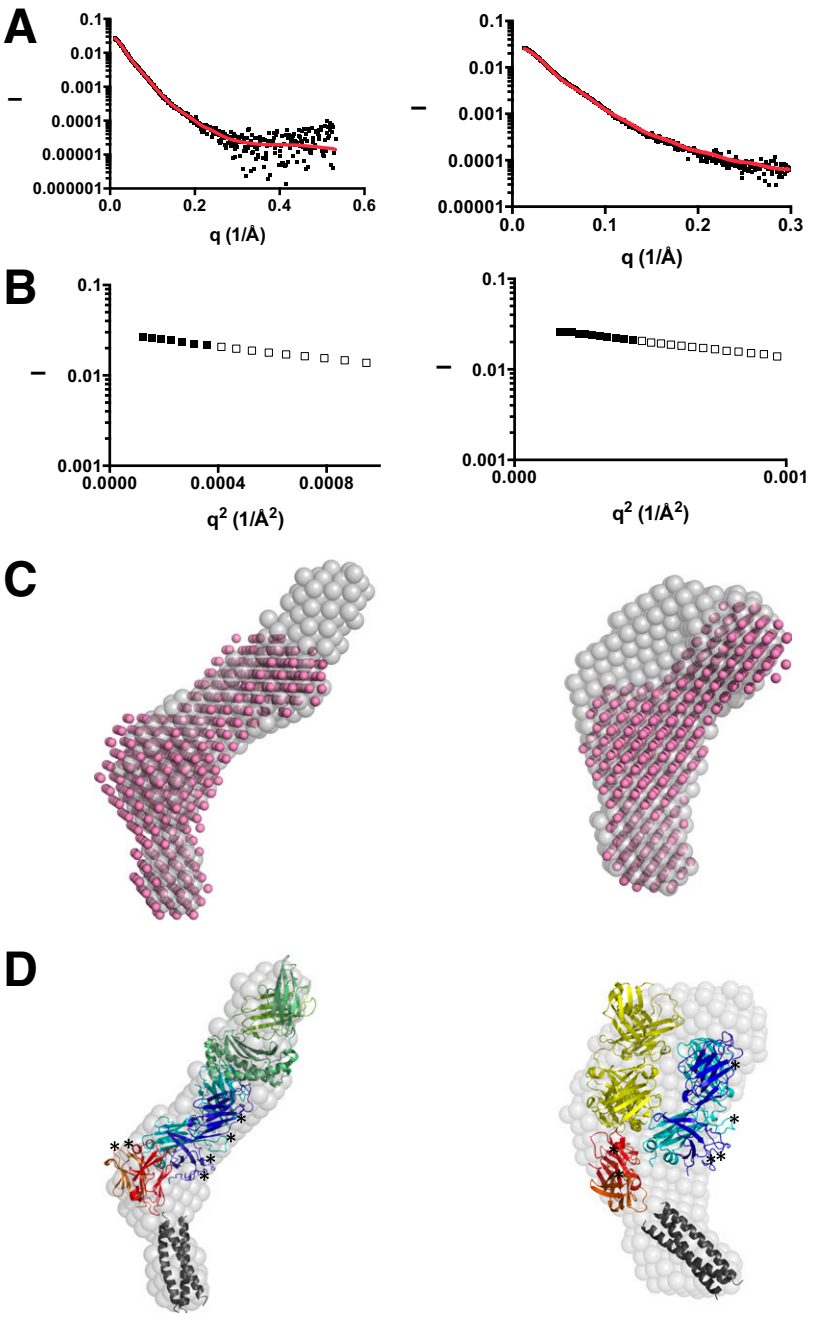

Fig. S3. Antibody/ligand mapping of LC13 TCR–CD3εδ. Scattering curves (*A*) and Guinier plots (*B*) are shown for LC13 TCR–CD3εδ in complex with HLA-B44 (*Left*) and the OKT3 Fab fragment (*Right*). In *B*, values of $q \leq 1/R_g$ are represented by filled squares. (*C*) The corresponding ab initio models derived from the SAXS data are shown in gray overlaid with that determined for LC13 TCR–CD3εδ alone (pink). The fit of the ab initio models (red line) to the raw SAXS data are shown in *A*. (*D*) Manual fit of the available high-resolution crystal structures (LC13–TCRα, blue; LC13–TCRβ, cyan; CD3ε, red; CD3δ, orange; coiled coil, gray; HLA-B44, green; OKT3, yellow) into the corresponding SAXS models. The previously determined interfaces (LC13–HLA-B44 and CD3ε–OKT3) have been retained.

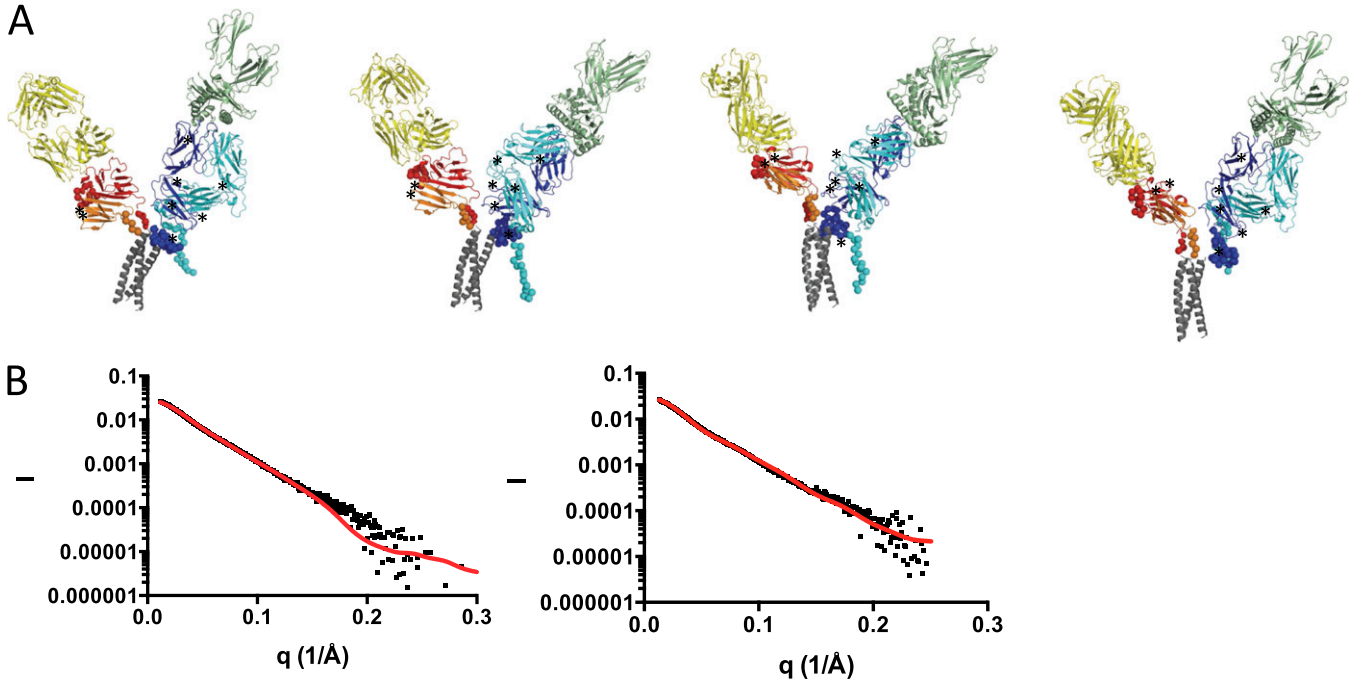

Fig. S4. (*A*) TCR–CD3–pMHC orientations as predicted through modeling with CORAL. Potential N-linked glycosylation sites in the TCR and CD3 subunits are indicated by asterisks. The fit of a representative model to the LC13 TCR–CD3εδ plus OKT3 (*Left*) and the LC13 TCR–CD3εδ plus HLA-B44 (*Right*) SAXS data are shown in *B*.

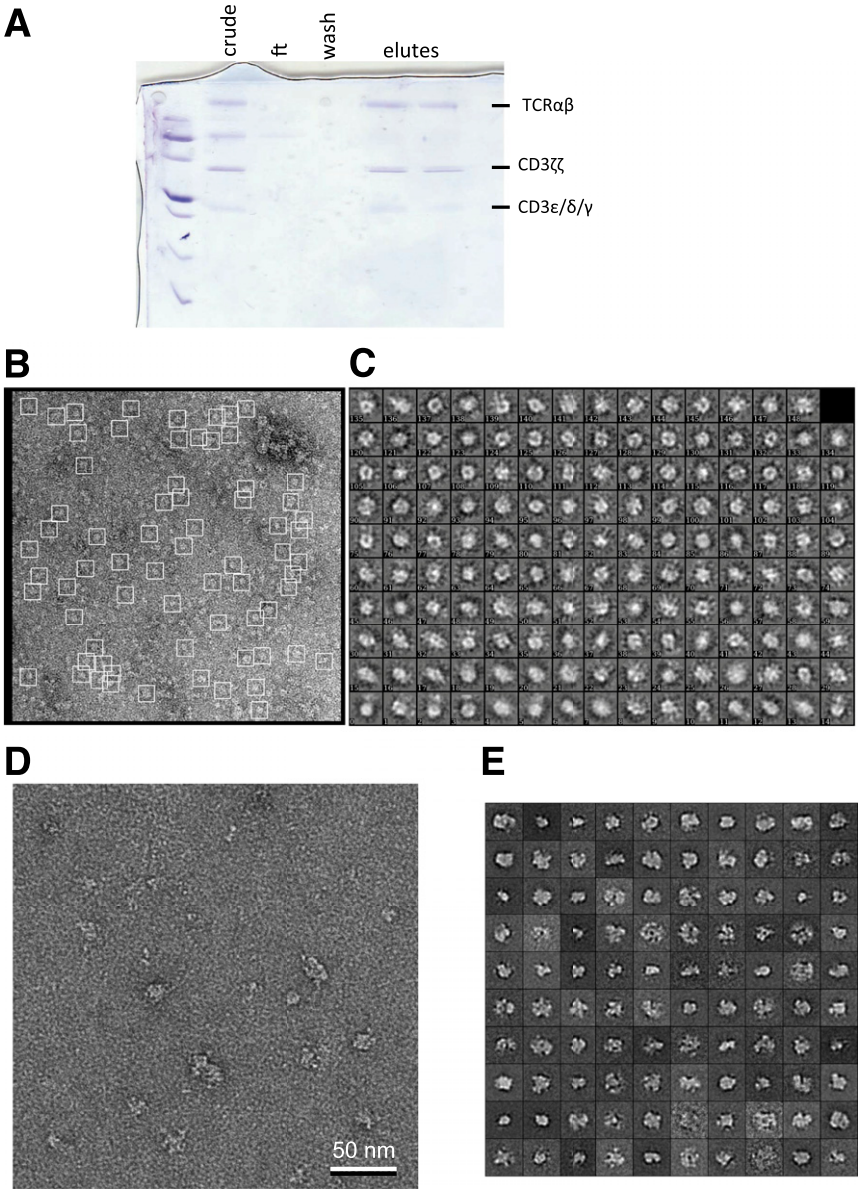

Fig. S5. Negative-stain EM of membrane-associated LC13 and 1G4 TCR–CD3 complex. (*A*) SDS-PAGE gel showing the presence of LC13 TCR and CD3 components. (*B*) Representative images of negatively stained LC13 TCR–CD3 complex. (*C*) The 2D class averages of LC13 TCR–CD3 particles (box size, 19.4 nm). (*D*) Representative images of negatively stained 1G4 TCR–CD3 complex. (*E*) The 2D class averages of 1G4 TCR–CD3 particles.

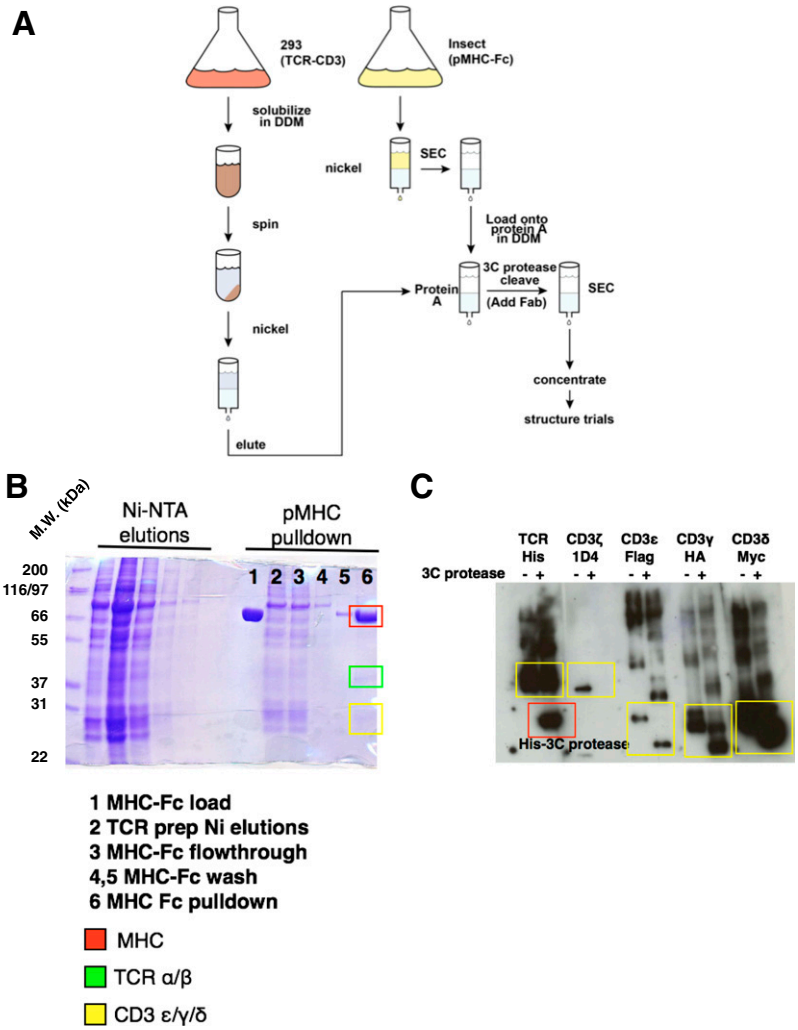

Fig. S6. (*A*) Tandem purification scheme for full-length 1G4 TCR–CD3 complex expressed in HEK-293 cells. (*B*) SDS-PAGE gel demonstrating initial Ni-NTA elutions of TCR–CD3 complex (*Left*) compared with pMHC purification (*Right*). (*C*) Western blot showing efficient cleavage of CD3 intracellular domains after Ni-NTA and pMHC purification steps via 3C protease cleavage of engineered protease sites. TCR is not cleaved as a result of lack of introduced protease sites. CD3ζ staining is lost because the antibody epitope is C-terminal to the protease site. The red box demonstrates the addition of 3C protease. Each protein product (labeled above) is highlighted with a yellow box. The 3C protease is His-tagged and is highlighted with a red box.

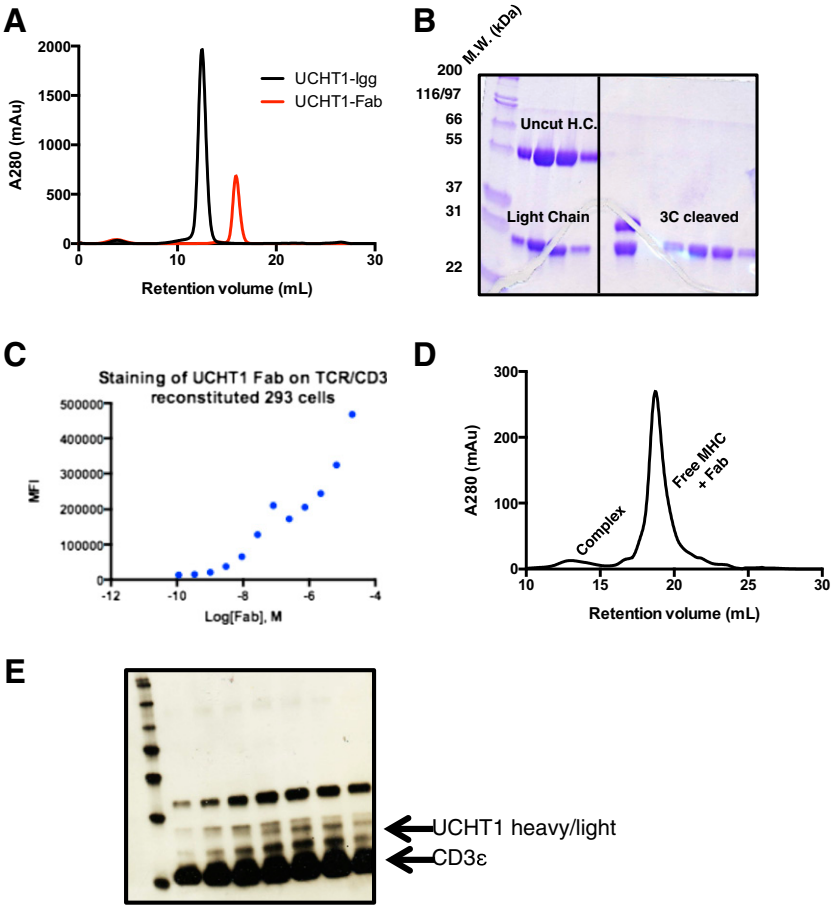

Fig. S7. Expression and characterization of UHCT1 Fab and cocomplex of UCHT1 with membrane-associated TCR–CD3 complex. Size-exclusion chromatography (*A*) and SDS-PAGE gel (*B*) of full-length UCHT1 antibody (black) and subsequently purified UCHT1 Fab (red). The UCHT1 antibody is expressed with an engineered 3C protease site between the Fab and Fc regions. (*C*) Titration of UCHT1 Fab on HEK-293 cells expressing 1G4 TCR–CD3. Size-exclusion chromatography (*D*) and Western blot (*E*) show cocomplex of UCHT1 Fab and membrane-bound 1G4 TCR–CD3–pMHC complex. Western blot stained with anti-Flag M2 (for CD3ε) and a polyclonal anti-mouse secondary antibody (to recognize M2 and the UCHT1 light and heavy chains).

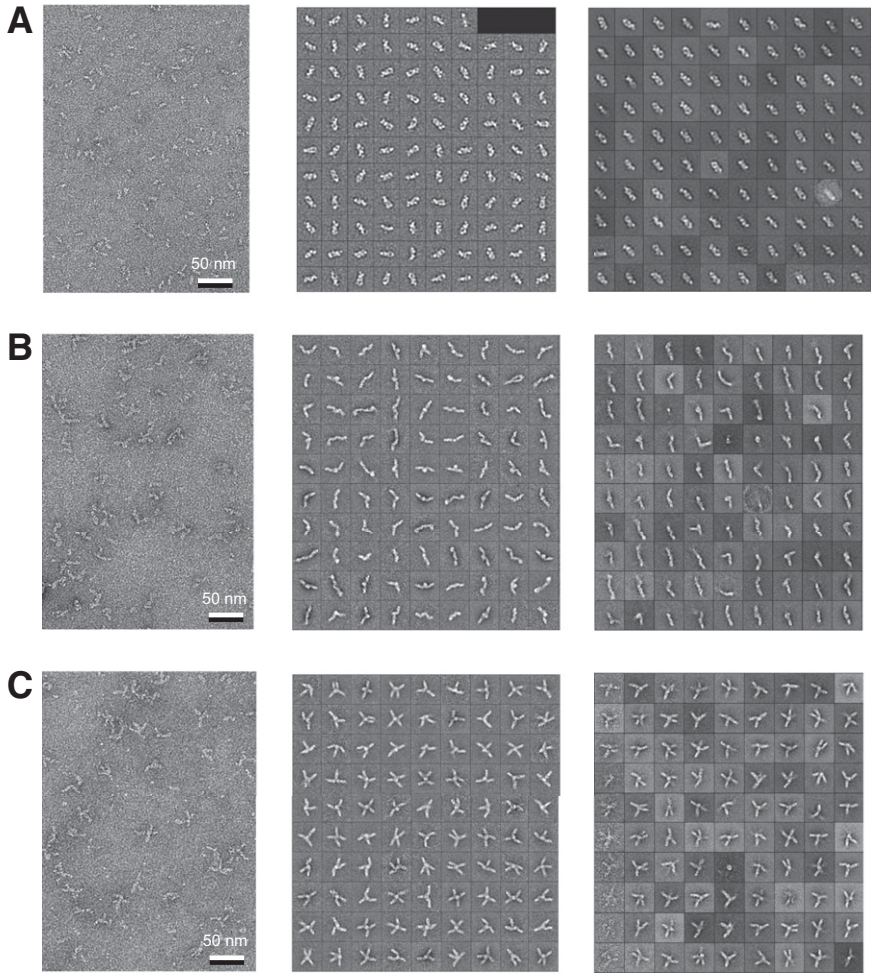

Fig. S8. Representative negative-stain EM images (*Left*) of full-length 1G4 TCR–CD3–pMHC complex (*A*), soluble 1G4 TCR–pMHC complex (*B*), and full-length 1G4 TCR–CD3–pMHC complex decorated with anti-CD3 Fab (*C*). Averages obtained by ISAC (*Center*) and K-means classification (*Right*) are provided for all species. The side length of the class averages in *A* is 25.6 nm, and the side length of the class averages in *B* and *C* is 42.6 nm.

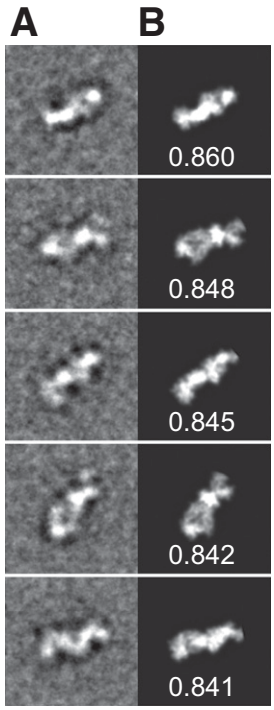

Fig. S9. Class averages of ESO–A2–1G4 TCR complexes (*A*) compared with the corresponding projections from a model based on the previously solved X-ray crystal structure (*B*) show good correlation (numbers in *B* represent correlation coefficient between EM averages and projections from the X-ray model).

Table S1. SAXS measurements

Sample	Concentration, mg/mL	R_g, Guinier, Å	R_g,Gnom, Å	MM, kDa	D_{max}, Å
CD3εδ	1.4	21.7	21.9	30	72
OKT3 Fab	2	26.3	26	57	77
	5	26.8	26.1	48	77
	10	28.1	26.6	50	80
LC13	3.65	25.4	25	46	72
	7.3	25.2	25	46	73
HLA-B8	2	24.7	24.4	86	72
	5	24.4	24.2	78	70
	10	24	23.8	69	70
LC13–CD3εδ	3	43.8	45.1	105	138
	6	43.4	44.4	106	140
LC13–CD3εδ + OKT3	ND	47.9	48.1	ND	140
LC13–CD3εδ + HLA-B44	ND	51	52.7	ND	180

D_{max}, maximal particle dimension; MM, molecular mass; ND, not determined.

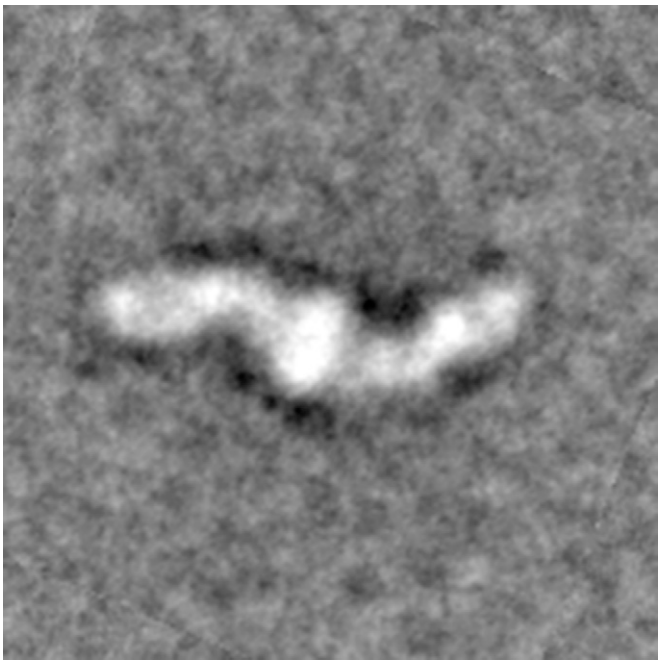

Movie S1. Collection of 2D class averages of pMHC–TCR–CD3 complex shows variability in orientation of pMHC–TCR ECD wings relative to the central CD3/TM region.

Movie S1

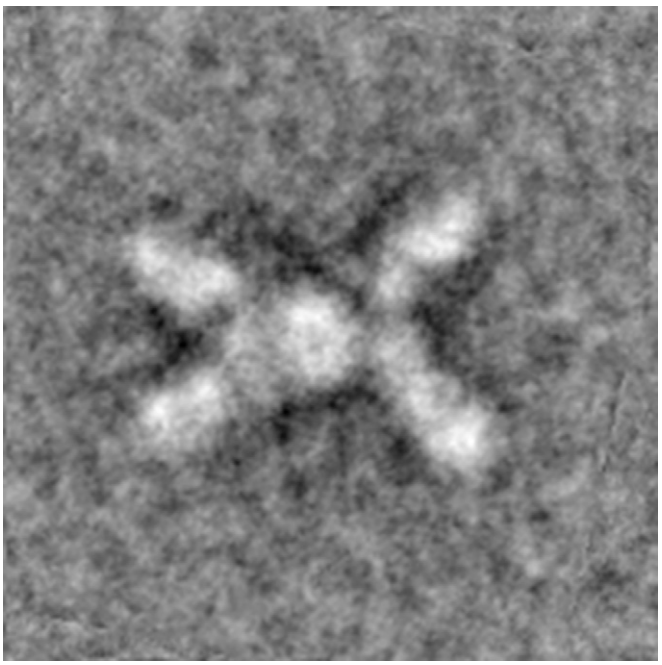

Movie S2. Collection of 2D class averages of Fab-decorated pMHC–TCR–CD3 complex shows variability observed in undecorated pMHC–TCR–CD3 complex is retained after binding of Fab.

Movie S2